International Journal of Research
Available at https://edupediapublications.org/journals
e-ISSN: 2348-6848
p-ISSN: 2348-795X
Volume 04 Issue14
November 2017

A Transformer less Upfc with Artificial Neural Network Controller

B. Divya Sree
Working as MATLAB developer and Branch Manager (DSNR) In Vision Krest Embedded Technologies, Private Ltd., Hyderabad

ABSTRACT- *Now a day's FACTS devices are used to control the flow of power, to increase the transmission capacity and to improve the stability of the power system. One of the most commonly used FACTS devices is Unified Power Flow Controller (UPFC)In this paper, a modulation and control method for the new transformer less unified power flow controller (UPFC) is presented. To overcome the problems with transformers, a completely transformer less UPFC based on an innovative configuration of two cascade multilevel inverters has been proposed. The new UPFC offers several advantages over the traditional technology, such as transformer less, light weight, high efficiency, low cost and fast dynamic response. This paper focuses on the modulation and control for this new transformer less UPFC, including artificial neural networks(ANN) controlling for low total harmonic distortion and high efficiency, independent active and reactive power control over the transmission line, dc-link voltage balance control, etc. Both the steady-state and dynamic response results will be shown in this paper. UPFC on controlling the flow of power and the effectiveness of controllers on the performance of UPFC is used to simulate UPFC model and to create the ANN.*

***Index Terms*-Flexible ac transmission systems (FACTS), artificial neural networks (ANN), unified power flow controller (UPFC).**

I. INTRODUCTION

The unified power flow controller (UPFC) is able to control, simultaneously or selectively, all the parameters affecting power flow in the transmission line (i.e., voltage magnitude, impedance, and phase angle) [1]–[3]. The conventional UPFC consists of two back-to-back connected voltage source inverters that share a common dc link, as shown in Fig. 1. The injected series voltage from inverter-2 can be at any angle with respect to the line current, which provides complete flexibility and controllability to control both active and reactive power flows over the transmission line. The resultant real power at the terminals of inverter-2 is provided or absorbed by inverter-1 through the common dc link. As a result, UPFC is the most versatile and powerful flexible ac transmission systems device. It can effectively reduce congestions and increase the capacity of existing transmission lines. This allows the overall system to operate at its theoretical maximum capacity. The basic control methods, transient analysis and practical operation considerations for UPFC have been investigated in [4]–[10].

The conventional UPFC has been put into several practical applications [11]–[13], which has the following features: 1) both inverters share the same dc link; 2) both Inverters need to exchange real power with each other and the transmission line; 3) a transformer must be used as an interface between the transmission line and each inverter. In addition, any utility-scale UPFC requires two high-voltage, high-power (from several MVA to hundreds of MVA) inverters. This high-voltage, high-power inverters have to use bulky and complicated zigzag transformers to reach their required VA ratings and desired voltage waveforms. The zigzag transformers are: 1) very expensive (30–40% of total system cost); 2) lossy (50% of the total power losses); 3) bulky (40% of system real estate area and 90% of the system weight); and 4) prone to failure [14]. Moreover, the zigzag transformer based UPFCs are still too slow in dynamic response due to large time constant of magnetizing inductance over resistance and pose control challenges because of transformer saturation, magnetizing current, and voltage surge [15].

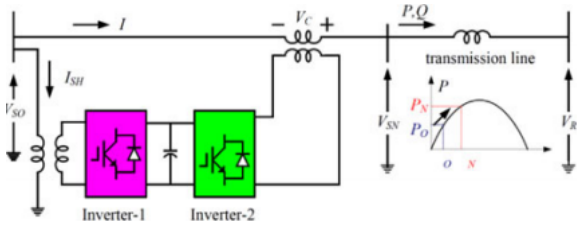

Fig. 1. Conventional UPFC.

Recently, there are two new UPFC structures under investigation: 1) the matrix converter-based UPFC [16]–[18] and 2) distributed power-flow controller (DPFC) derived from the conventional UPFC [19]. The first one uses the matrix converter replacing the back-to-back inverter to eliminate the dc capacitor with ac capacitor on one side of the matrix converter. The DPFC employs many distributed series inverters coupled to the transmission line through single-turn transformers and the common dc link between the shunt and series inverters is eliminated. The single-turn transformers lose one design freedom, thus making them even bulkier than a conventional transformer given a same VA rating. In summary, both UPFCs still have to use the transformers, which inevitably cause the same aforementioned problems associated with transformers (such as bulky, lossy, high cost, and slow in response).

The cascade multilevel inverter (CMI) is the only practical inverter technology to reach high voltage levels without the use of transformers, a large number of semiconductor devices (diodes), or a large number of capacitors [14], [20]–[22]. The CMI-based STATCOMs (up to ±200 Mvar) have been installed in Europe and Asia [23]–[25]. However, the CMI could not be directly used in the conventional UPFC, because the conventional UPFC requires two inverters connected back-to-back to deal with active power exchange. To address this problem, a UPFC with two face-to-face connected CMIs was developed in [26] to eliminate the zigzag transformers that are needed in the conventional multi pulse inverter-based UPFC. However, it still required an isolation transformer.

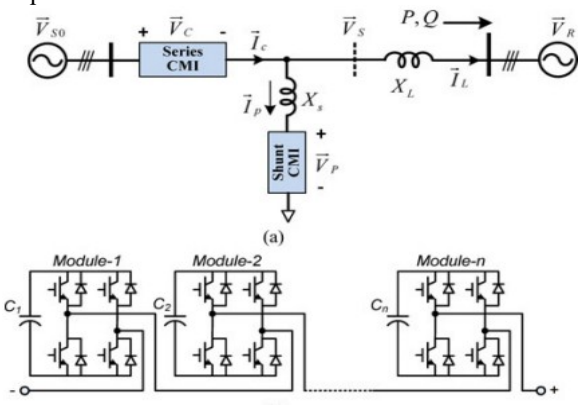

Fig. 2. New transformer less UFPC. (a) System configuration of transformer less UPFC. (b) One phase of the cascaded multilevel inverter.

To eliminate the transformer completely, a new transformer less UPFC based on an innovative configuration of two CMIs has been proposed in [27]. The system configuration is shown in Fig. 2(a) and main system parameters for a 13.8-kV/2-MVA prototype (target system) is shown in Table I. As shown in Fig. 2(a), the transformer less UPFC consists of two CMIs, one is series CMI, which is directly connected in series with the transmission line; while the other is shunt CMI, which is connected in parallel to the sending end after series CMI. Each CMI is composed of a series of cascaded H-bridge modules as shown in Fig. 2(b).

TABLE I
MAIN SYSTEM PARAMETERS FOR 13.8-KV PROTOTYPE

Parameters	Value
System power rating	2 MVA
V_{s0} rms	13.8 kV
Max series CMI current, I_C rms	84 A
Max shunt CMI current, I_P rms	42 A
V_{dc} (Shunt)	600 V
V_{dc} (Series)	600 V
H-bridge dc capacitance	2350 μF
No. of H-bridges per phase (Shunt)	20
No. of H-bridges per phase (Series)	10

The transformer less UPFC has significant advantages over the traditional UPFC such as highly modular structure, light weight, high efficiency, high reliability, low cost, and a fast dynamic response. The basic operation principle, operation range, and required VA rating for series and shunt CMIs have been studied in [27]. Nevertheless, there are still challenges for the modulation and control of this new UPFC: 1) UPFC power flow control, such as voltage regulation, line impedance compensation, phase shifting or simultaneous control ofvoltage, impedance, and phase angle, thus achieving independently control both the active and reactive power flow in the line; 2) dc capacitor voltage balance control for H-bridges of both series and shunt CMIs; 3) modulation of the CMI for low total harmonic distortion (THD) of output voltage and low switching loss; 4) fast system dynamic response. This paper presents the modulation and control for the new transformer less UPFC to address aforementioned challenges. The UPFC functionality
with proposed control method is verified at low voltage level (4160 V), and both the steady-state and dynamic responses results will be shown in this paper.

Work on ANN or a simply neural network has been motivated right from its inception by the recognition that the human brain computes in an entirely different way from the conventional digital computer [28]. In recent past years there has been a confluence of ideas and methodologies from several disciplinary areas to give rise to an extremely interesting research area known as ANN [29]. ANNs are parallel computational models comprised of densely interconnected adaptive processing units, called neurons. It is due to this adaptive nature, where learning by experience replaces programming in solving problem. This feature makes such computational models very appealing in application domains where one has little or incomplete understanding of the problem to be solved but where training data is readily available [30]. The biggest advantage of ANN is that it is a high speed online computational technique, which once trained through an offline algorithm using example patterns, can provide an

International Journal of Research
Available at https://edupediapublications.org/journals
e-ISSN: 2348-6848
p-ISSN: 2348-795X
Volume 04 Issue14
November 2017

output corresponding to a new pattern without any iteration in real time [31].

II. OPERATION PRINCIPLE OF THE TRANSFORMER LESS UPFC

With the unique configuration of the series and shunt CMIs, the transformer less UPFC has some new features:
1) Unlike the conventional back-to-back dc link coupling, the transformer less UPFC requires no transformer, thus it can achieve low cost, light weight, small size, high efficiency, high reliability, and fast dynamic response.
2) The shunt inverter is connected after the series inverter, which is distinctively different from the traditional UPFC. Each CMI has its own dc capacitor to support dc voltage.
3) There is no active power exchange between the two CMIs and all dc capacitors are floating.
4) The new UPFC uses modular CMIs and their inherent redundancy provides greater flexibility and higher reliability.

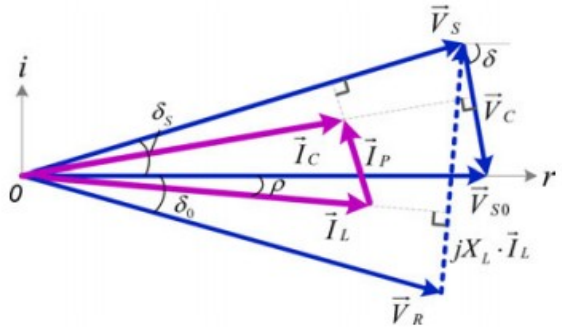

Fig. 3. Phasor diagram of the transformer less UPFC.

Due to the unique system configuration, the basic operation principle of the transformer less UPFC is quite different from conventional UPFC. Fig. 3 shows the Phasor diagram of the transformer less UPFC, where $\vec{V}_{SO}$ and $\vec{V}_R$ are the original sending-end and receiving-end voltage, respectively. Here, $\vec{V}_{SO}$ is aligned with real axis, which means phase angle of $\vec{V}_{SO}$ is zero. The series CMI is controlled to generate a desired voltage $\vec{V}_C$ for obtaining the new sending-end voltage $\vec{V}_S$, which in turn, controls active and reactive power flows over the transmission line. Meanwhile, the shunt CMI injects a current $\vec{I}_p$ to the new sending-end bus to make zero active power into both CMIs, i.e., to make the series CMI current $\vec{I}_C$ and the shunt CMI current $\vec{I}_p$ be perpendicular to their voltages $\vec{V}_C$ and $\vec{V}_S$, respectively. As a result, both series and shunt CMIs only need to provide the reactive power. In such a way, it is possible to apply the CMIs to the transformer less UPFC with floating dc capacitors for H-bridge modules.

The detailed operating principle of the transformer less UPFC can be formulated as follows. With referring to Figs. 2 and 3, the transmitted active power P and reactive power Q over the line with the transformer-less UPFC can be expressed as:

$$P + jQ = \vec{V}_R.\left(\frac{\vec{V}_{SO} - \vec{V}_C - \vec{V}_R}{jX_L}\right)^*$$
$$= \left(\frac{V_O V_R}{X_L}\sin\delta_O + \frac{V_c V_R}{X_L} sin(\delta_O - \delta)\right)$$
$$+j\left(\left(\frac{V_{SO} V_R \cos\delta_O - V_R^2}{X_L} - \frac{V_c V_R}{X_L}\cos(\delta_O - \delta)\right)\right) \quad (1)$$

Where, symbol $*$ represents the conjugate of a complex number; δ_0 is the phase angle of the receiving-end voltage $\vec{V}_R$; δ is the phase angle of the series CMI injected voltage $\vec{V}_C$; X_L is the equivalent transmission line impedance. The original active and reactive powers, P_0 and Q_0 with the uncompensated system (without the UPFC, or $V_C = 0$) are

$$\begin{cases} P_O = -\frac{V_{SO}V_R}{X_L} sin\delta_O \\ Q_O = \frac{V_{SO}V_R \cos\delta_O - V_R^2}{X_L} \end{cases} \quad (2)$$

The net differences between the original (without the UPFC) powers expressed in (2) and the new (with the UPFC) powers in (1) are the controllable active and reactive powers, P_C and Q_C by the transformer less UPFC, which can be expressed as

$$\begin{cases} P_C = \frac{V_C V_R}{X_L}\sin(\delta_0 - \delta) \\ Q_C = -\frac{V_C V_R}{X_L}\cos(\delta_0 - \delta) \end{cases} \quad (3)$$

Therefore, we can rewrite (1) as

$$P + jQ = \left(-\frac{V_{S0}V_R}{X_L}\sin\frac{\delta_0}{P_0} + \frac{\frac{V_C V_R}{X_L}\sin(\delta_0 - \delta)}{P_c}\right)$$
$$+ j\left(\frac{V_{S0}V_R\cos\delta_0 - V_R^2}{X_L}/Q_0 - \frac{V_C V_R}{X_L}\cos(\delta_0 - \delta)/Q_c\right) \quad (4)$$

Because both amplitude V_C and phase angle δ of the UPFC injected voltage $\vec{V}_C$ can be any values as commanded, the new UPFC provides a full controllable range of $(-V_C V_R/X_L)$ to $(+V_C V_R/X_L)$ for both active and reactive powers, P_C and Q_C, which are advantageously independent of the original sending end voltage and phase angle δ_0. In summary, (1)–(4) indicate that the new transformer less UPFC has the same functionality as the conventional UPFC.

International Journal of Research
Available at https://edupediapublications.org/journals
e-ISSN: 2348-6848
p-ISSN: 2348-795X
Volume 04 Issue14
November 2017

In summary, (1)–(4) indicate that the new transformer less UPFC has the same functionality as the conventional UPFC. First, the series CMI voltage $\vec{V}_C$ is injected according to transmission line active/reactive power command, which can be calculated from (3).

$$\vec{V}_C = V_C\angle\delta = \frac{X_L}{V_R}\sqrt{P_c^2+Q_C^2}\ \angle\left(\delta_0 - arctan\left(\frac{P_C}{Q_C}\right)\right) \quad (5)$$

Once the series CMI injected voltage $\vec{V}_C$ is decided by (5), the new sending-end voltage $\vec{V}_S$ and the transmission line current will be decided accordingly

$$\vec{V}_S = V_S\angle\delta_S = \vec{V}_{s0} - \vec{V}_C \quad (6)$$

Where,

$$\begin{cases} V_s = \sqrt{(V_{S0} - V_C\cos\delta)^2 + (V_C\sin\delta)^2} \\ \delta_s = arctan\left(\frac{-V_C\sin\delta}{V_{S0}-V_C\cos\delta}\right) \end{cases} \quad (7)$$

And

$\vec{I}_L = I_L\angle\rho$, where

$$I_L = \frac{\sqrt{(V_C\sin\delta + V_R\sin\delta_0)^2 + (V_{S0} - V_C\cos\delta - V_R\cos\delta_0)^2}}{I_L}$$

$$\rho = \arctan\left(\frac{V_{S0} - V_C\cos\delta - V_R\cos\delta_0}{V_C\sin\delta + V_R\sin\delta_0}\right) \quad (8)$$

Next, the shunt CMI injects current $\vec{I}_p$ to decouple the series CMI current $\vec{I}_C$ from the line current $\vec{I}_L$. In such a way, zero active power exchange to both series and shunt CMIs can be achieved, making it possible to apply the CMI with floating capacitors to the proposed transformer less UPFC. Therefore, we have

$$\begin{cases} P_{se} = \vec{V}_C.\vec{I}_C = 0 \\ P_{sh} = \vec{V}_S.\vec{I}_p = 0 \end{cases} \quad (9)$$

It means the series CMI current $\vec{I}_c$ and the shunt CMI current $\vec{I}_p$ need to be perpendicular to their voltages $\vec{V}_C$ and $\vec{V}_S$, respectively, as illustrated in Fig. 3. With the geometrical relationship of the voltages and currents in Fig. 3, the shunt CMI output current can be calculated as

$$\vec{I}_P = I_P\angle\theta_{Ip} \quad (10)$$

Where,

$$\begin{cases} I_P = I_L\left(\frac{\cos(\rho-\delta_S)}{\tan(\rho-\delta_S)} - \sin(\rho-\delta_S)\right) \\ \theta_{Ip} = 90 + \delta_S \end{cases} \quad (11)$$

In summary, there are two critical steps for the operation of UPFC: 1) calculation of injected voltage $\vec{V}_C$ for series CMI according to active/reactive power command over the transmission line expressed in (5), and 2) calculation of injected current IP for shunt CMI from (10) and (11) to guarantee zero active power into both series and shunt CMIs.

III. FUNDAMENTAL FREQUENCY MODULATION (FFM) FOR CMIS

Before embarking on development of UPFC control, the modulation strategy for CMIs is introduced first. In general, the modulation for CMIs can be classed into two main categories: 1) FFM and 2) carrier-based high-frequency pulse width modulation (PWM). Compared to the carrier-based high-frequency PWM, the FFM has much lower switching loss, making it attractive for the transmission-level UPFC and other high-voltage high-power applications.

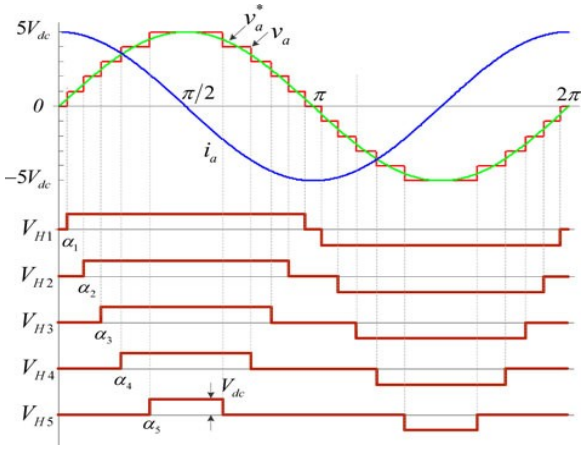

Fig. 4. Operation principle of FFM.

A. Optimization of Switching Angles for Minimum THD

Fig. 4 shows the operation principle of traditional FFM, where phase *a* output voltage of an 11-level CMI is shown as an example. A stair-case voltage waveform, *Va* could be synthesized when each of five H-bridge modules generates a quasi-square wave, *VH*1, *VH*2, . . . , *VH*5 . Each H-bridge has the identical dc link voltage *V*dc for the modular design consideration.

The Fourier series expansion of the CMI output voltage shown in Fig. 4 is

International Journal of Research
Available at https://edupediapublications.org/journals
e-ISSN: 2348-6848
p-ISSN: 2348-795X
Volume 04 Issue14
November 2017

$$V_a(\omega t) = \sum_{n=1}^{\infty} V_{an}.\sin(n\omega t),$$

$$V_{an} = \begin{cases} \frac{4}{n\pi}\sum_{k=1}^{s} V_{an}.\cos(n\alpha_k), & foroddn \\ 0, & forevenn \end{cases} (12)$$

Where n is harmonic number, s is the total number of H-bridge modules, and αk represents the switching angle for the kth H-bridge module. Therefore, all triplen harmonics will be ignored for voltage THD calculation which then can be expressed as

$$THD = \frac{1}{V_{a1}}\sqrt{\sum_{n=5,7,11....}^{\infty} V_{an}^2} (13)$$

Basically, (13) gives an objective function to be minimized, with the following two constraints:

$$0 < \alpha_1 < \alpha_2 < \alpha_3 \ldots\ldots < \alpha_s < \frac{\pi}{2} (14)$$

And

$$V_{a1} = \frac{4}{\pi}\sum_{k=1}^{s} V_{dc}\cos(\alpha_k) (15)$$

The corresponding results have been shown in Fig. 5.

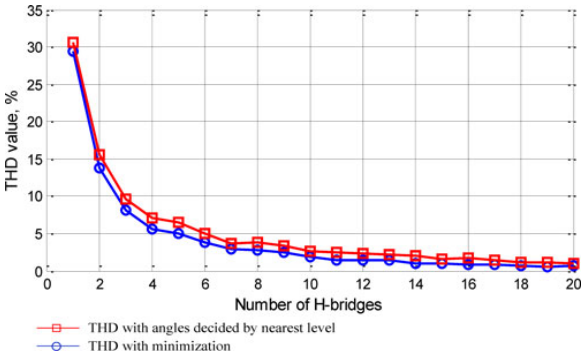

Fig. 5. Minimum THD versus number of H-bridge modules.

In addition, an alternative optimization of FFM could be the "minimum weighted total harmonics distortion (WTHD)." The WTHD achieves the minimum current THD for inductive loads (i.e., directly optimized for best power quality), which is preferred for application where current distortion is of interest. In such a case, the objective function in (13) should be changed to

$$WTHD = \frac{1}{v_{a1}}\sqrt{\sum_{n=5,7,11....}^{\infty}(V_{an}/n)^2} (16)$$

As shown in Table I, for the 13.8-kV/2-MVA system, the number of H-bridges for shunt CMI is ten and the number of H-bridges for series CMI is 20.

The corresponding optimized switching angles for this case are given in Table II.

In summary, compared to carrier-based high-frequency PWM scheme, the CMIs with FFM have the following features:

1) FFM has much lower switching loss, thus higher efficiency;

2) With high number of H-bridge modules, output voltage could be very close to sinusoidal;

3) It is notable that FFM does not actually mean slow dynamic response. With high-frequency sampling, FFM can also achieve fast dynamic response, e.g., <10 ms, which will be discussed and experimentally verified in the next section.

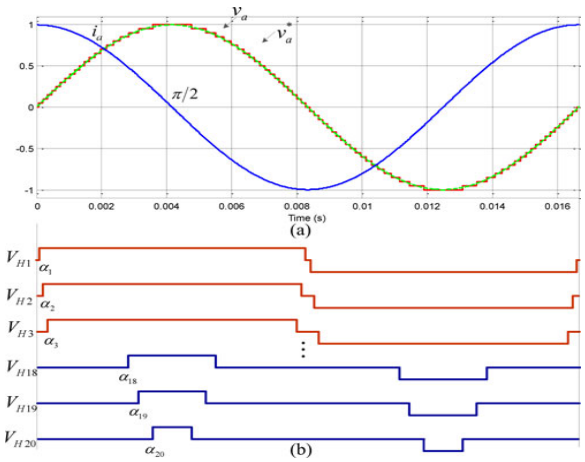

Fig. 6. FFM with total 20 H-bridges. (a)Output voltage and current (41 levels) and (b) output voltage of each H-bridge.

B. Analysis of Capacitor Charge of H-Bridges

Capacitor charge of H-bridges will be studied based on two layers: 1) first layer is overall capacitor charge, meaning the total capacitor charge of all H-bridges of any one of three phases; 2) the other layer is individual capacitor charge, meaning the capacitor charge of each H-bridge. The overall active power flow of this phase from ac side into dc capacitors can be expressed as

$$P_a = V_0 I_0.\cos(\theta) (17)$$

Where, Vo and Io are rms values of CMI output phase voltage and current, respectively, and θ is the phase angle between output voltage and current. However, if the phase angle θ is smaller than 90°, denoted as(90◦ − Δθ), the overall dc capacitor voltage could be balanced if

$$P_a = V_0 I_0.\cos(90 - \Delta\theta) = V_0 I_0.\sin(\Delta\theta) = P_{loss} (18)$$

International Journal of Research
Available at https://edupediapublications.org/journals
e-ISSN: 2348-6848
p-ISSN: 2348-795X
Volume 04 Issue14
November 2017

Where, Ploss is the total power loss of switching devices and capacitors of one phase. On the other side, with the shifted phase angle$\Delta\theta$, the individual capacitor charge for kth H-bridge, Ck over one fundamental period is given as

$$C_k = \int i_{dc}dt = \frac{2}{\omega}.\int_{\alpha_k-\Delta\theta}^{\pi-\alpha_k-\Delta\theta} \sqrt{2}I_0\cos(\theta)d\theta = 4\omega 2I0\cos\alpha k\sin\Delta\theta \quad (19)$$

Where, k = 1, 2, . . . , s. In (19), the entire modules in the same phase will have same load current Io and phase angle shift $\Delta\theta$. (19) indicates the quite different individual capacitor charge due to the unequal duty cycles of H-bridge modules. Fig. 7 illustrates the capacitor charges of 20 shunt H bridges with corresponding switching angles given in Table II.When the same load current go through all these 20 H bridges, dc capacitor of each H bridge will be charged differently. One important point here is, the smaller switching angle (corresponding to larger duty cycle) an H-bridge module has, the more capacitor charge it will get.

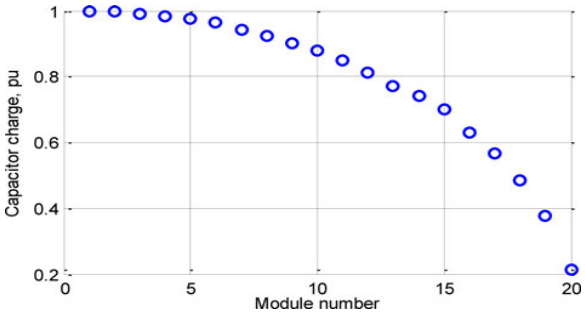

Fig. 7. Capacitor charge of 20 H-bridge modules with FFM.

IV. POWER FLOW AND DC-LINK VOLTAGE CONTROL OF TRANSFORMER LESS UPFC

A. Dynamic Models of UPFC System

In order to design the vector-oriented control for the proposed transformer less UPFC with considering both steady-state and dynamic performance, the dynamic modules are necessary. The models are based on synchronous (dq) reference frame. The phase angle of original sending-end voltage Vs0 is obtained from a digital phase-locked loop, which is used for abc to dq transformation. The dynamic models for the whole system shown in Fig. 2(a) will be divided into several parts. First, we can get the dynamic model from the new sending-end bus to receiving-end bus

$$\begin{cases} V_{sd} = R_L i_{Ld} + L_L \frac{di_{Ld}}{dt} - \omega L_L i_{Lq} + V_{Rd} \\ V_{sq} = R_L i_{Lq} + L_L \frac{di_{Lq}}{dt} - \omega L_L i_{Ld} + V_{Rq} \end{cases} \quad (20)$$

Since the new sending-end voltage v_s is equal to original sending-end voltage v_{s0} minus series CMI injected voltage v_c, thus we have

$$\begin{cases} V_{cd} = V_{S0d} - V_{Sd} \\ V_{cq} = V_{S0q} - V_{Sq} \end{cases} \quad (21)$$

Furthermore, the model from the new sending-end to shunt CMI is

$$\begin{cases} V_{sd} = R_s i_{pd} + L_s \frac{di_{pd}}{dt} - \omega L_s i_{pq} + V_{pd} \\ V_{sq} = R_s i_{pq} + L_s \frac{di_{pq}}{dt} - \omega L_s i_{Pd} + V_{pq} \end{cases} \quad (22)$$

B. Power Flow and Overall DC Voltage Control

It is desired to design a control system, which can independently regulate the active power *P* and reactive *Q* in the line, at the same time, maintain the capacitor voltages of both CMIs at the given value. Fig. 8(a) shows the overall control system, which is divided into three stages, i.e., stage I to stage III.

Stage I: The calculation from P^*/Q^* to $\overrightarrow{V}^*_{C0}$ and $\overrightarrow{I}^*_{p0}$. As mentioned before, the $\overrightarrow{V}^*_{C0}$ is the voltage reference for series CMI, which is generated according to the transmission line power command as given in (5), while $\overrightarrow{I}^*_{p0}$ current reference for shunt CMI, which is used to keep zero active power for both CMIs as given in (10), (11). Note that instead of calculating $\overrightarrow{V}^*_{C0}$ directly from (5), an alternative way is shown in Fig. 8(b). Here, the line current reference I^*Ld/I^*Lq is calculated out of the P^*/Q^* reference, then the d- and q-axis components of series voltage V^*_{C0d}, V^*_{C0q} are calculated according to (23), where the dynamic model of (20) is included. The line current is controlled in a way of decoupling feed forward control, thus better line current dynamic response could be achieved.

$$V^*_{C0d} = V_{S0d} - V^*_{Sd} = V_{S0d} - (R_L I^*_{Ld} + L_L dI^*_{Ld}/dt - \omega L_L I^*_{Lq} + V_{Rd})$$
$$V^*_{C0q} = V_{S0q} - V^*_{Sq} = V_{S0q} - (R_L I^*_{Lq} + L_L dI^*_{Lq}/dt + \omega L_L I^*_{Ld} + V_{Rq}) \quad (23)$$

Stage II: overall dc-link voltage regulation. With the $\overrightarrow{V}^*_{C0}$ and $\overrightarrow{I}^*_{p0}$ given in stage I, the dc-link voltage cannot be maintained due to the following three main reasons: 1) the CMIs always have a power loss, 2) the calculation error caused by the parameter deviations, 3) the error between reference and actual output. In order to control dc-link voltage with better robustness, two

International Journal of Research
Available at https://edupediapublications.org/journals
e-ISSN: 2348-6848
p-ISSN: 2348-795X
Volume 04 Issue14
November 2017

variables $\Delta\vec{V}_C$ and $\Delta\vec{I}_p$ were introduced for the independent dc-link voltage regulation of series CMI and shunt CMI, respectively, as shown in Fig. 8(a). In this figure, V^*_{dcsh} and V^*_{dcse} aredc voltage references for shunt and series CMIs, respectively; V_{dcsh} and V_{dcse} are the averaged dc feedback of shunt and series CMIs, respectively. For the series CMI, P_{se} is the output of overall dc-link voltage regulation loop, R_{se} is then calculated by dividing P_{se} by I^2_C (square of rms value of series CMI current), finally $\Delta\vec{V}_C$is the product of R_{se} and series CMI current $\vec{I}_C$.

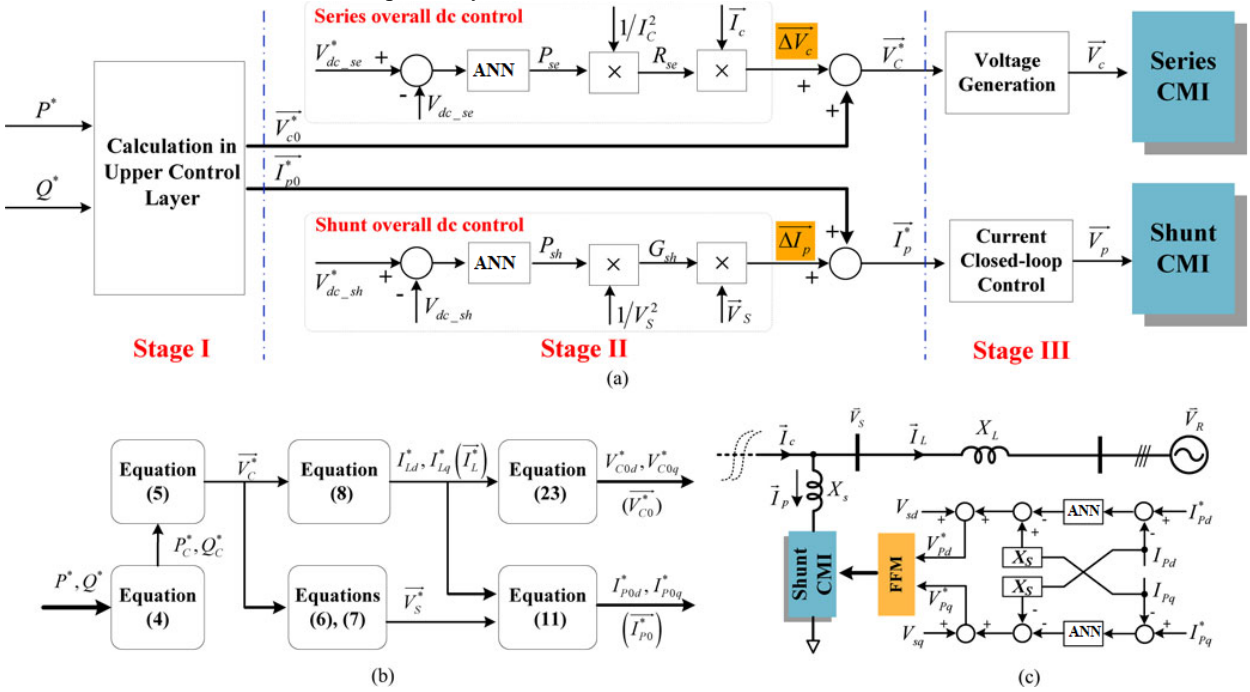

Fig. 8. Control system for transformerless UPFC. (a) Overall control diagram for power flow and dc capacitor voltage control, (b) detailed calculation from P^*/Q^* to $\vec{V}^*_{C0}$ and $\vec{I}^*_{p0}$, and (c) current closed-loop control for shunt CMI.

Obviously, the introduced $\Delta\vec{V}_C$is always in phase with series CMI$\vec{I}_C$, which can be regarded as *active voltage* component. Basically,*Rse* is the equivalent resistance of series CMI, and the dc-link can be balanced when *Pse* is equal to *P*loss (total power loss of series CMI). For the shunt CMI, $\Delta\vec{I}_p$is introduced for the dc-link voltage control in a similar way.

Stage III: voltage and current generation for series and shunt CMI, respectively. For series CMI, output voltage could be directly generated from the reference$\vec{V}^*_C$by FFM. While for shunt CMI, decoupling feedback current control is used to control output current to follow the reference current $\vec{I}^*_p$, as shown in Fig. 8 (c) [22].

C. Individual DC Control and Phase Balance Control

Usually, the dc capacitor voltage balance control for CMIs adopts hierarchical control structure, e.g., an outer control loop and an inner control loop. The outer loop regulates the overall active power flowing to all H-bridge modules of any one of three phases, while the inner loop distributes power flowing equally to each individual H-bridge module [22]. As we discussed in Section III, one fact is that the capacitor charge of individual H-bridge will be unequal due to the unequal duty cycles of each H-bridge by FFM. The smaller switching angle (corresponding to larger duty cycle) an H-bridge module has, the more capacitor charge it will get. Besides the overall dc capacitor voltage control present above, it is necessary to have the individual dc capacitor voltage control for the charge balance between the modules in the same phase.

Even with both overall and individual dc capacitor voltage control described above, it is still possible to have the dc capacitor voltage unbalance between the three phases. Physically, the shunt CMI or series CMI may have different power loss between the three phases. If same *Psh/Pse* from overall dc voltage regulator is applied to all three phases of shunt/series CMI as shown in Fig. 8(a), the mismatch between the absorbed active power and the power loss would cause the voltage unbalance. One simple solution to this problem is to

International Journal of Research
Available at https://edupediapublications.org/journals
e-ISSN: 2348-6848
p-ISSN: 2348-795X
Volume 04 Issue14
November 2017

change the overall dc voltage control in Fig. 8(a) from one three-phase integrated controller to three separated controllers as shown in Fig. 10, where $V_{dc\ sea}$, $V_{dc\ seb}$, and $V_{dc\ sec}$ are dc capacitor voltage feedback of phase *a*, *b*, and *c*, respectively; P_{se_a}, P_{se_b}, P_{se_c} are active power commands, which are used to compensate the power loss of each phase; i_{c_a} , i_{c_b} and i_{c_c} are instantaneous currents of each phase of series CMIs; Δv_{ca}, Δv_{cb}, Δv_{cc} are generated as the *active-voltage* components, which are in phase with current i_{c_a}, i_{c_b} and i_{c_c}, respectively.

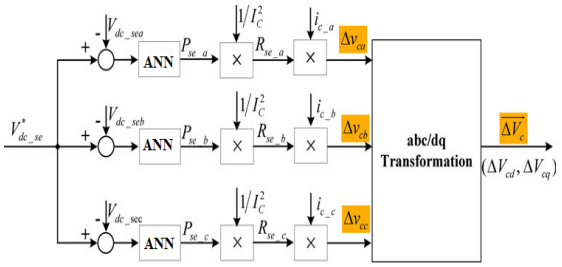

Fig. 10. Three-phase separated overall dc voltage control for series CMI, considering capacitor-voltage unbalance between the three phases.

In a three-phase well balanced system, P_{se_a}, P_{se_b}, P_{se_c} will be close to each other, indicating the same active power is needed to compensate the power loss of each phase; while in a system with different power losses between three phases, the separated dc regulators will output different value of P_{se_a}, P_{se_b} and P_{se_c} to guarantee the balanced dc capacitor voltage. It is notable that the value of P_{se_a}, P_{se_b} and P_{se_c} are relatively small when compared to the total UPFC system rating. Similarly, from Fig. 8(a) we can derive the corresponding three-phase separated overall dc voltage control for shunt CMI.

IV. ARTIFICIAL NEURAL NETWORKS

An artificial neural network is made of up connections of simple processing units (neurons). The basic neural network architecture consists of an input layer, one or more middle or hidden layers for processing and computation, and an output layer. The number of neurons in the first input layer is equivalent to the number of inputs into the system. Each input neuron having only one source. The number of hidden layers and the number of neurons per hidden layer are user defined for the processing abilities needed by the specific system. The number of neurons in the output layer corresponds to the number of outputs from the controller. A single neuron can have multiple input connections aswell as multiple connections to the next neural layer. In our case, we will only describe the structure, mathematics and behavior of that structure known as the backpropagation network. This is the most prevalent and generalized neural network currently in use. To build a backpropagation network, proceed in the following fashion. First, take a number of neurons and array them to form a layer. A layer has all its inputs connected to either a preceding layer or the inputs from the external world, but not both within the same layer.

A layer has all its outputs connected to either a succeeding layer or the outputs to the external world, but not both within the same layer. Next, multiple layers are then arrayed one succeeding the other so that there is an input layer, multiple intermediate layers and finally an output layer, as in Figure 3. Intermediate layers, that is those that have no inputs or outputs to the external world, are called >hidden layers. Back propagation neural networks are usually fully connected. This means that each neuron is connected to every output from the preceding layer or one input from the external world if the neuron is in the first layer and, correspondingly, each neuron has its output connected to every neuron in the succeeding layer. Generally, the input layer is considered a distributor of the signals from the external world. Hidden layers are considered to be categorizers or feature detectors of such signals. The neural network works according to the Eqn.24.

$$Y_i = \sum_{j=1}^{N} (W_{ij} X_j) \qquad (24)$$

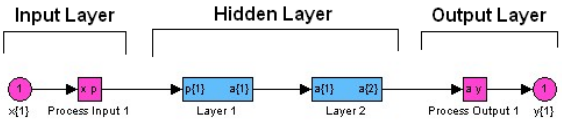

Fig. 11. Artificial Neural Network Block Diagram

The above figure 11 represents the general block diagram designed using Simulink. It consists of one input layer (process input 1), two hidden layers (layer 1, layer 2) and one output layer (process output 1).The input layer collects data from a source. For this controller, the input data is the error calculated via the feedback. Each network has only a single neuron in the first layer because there is only one input data value per side. The two hidden layers provide the main computational processing (Figure 12). The first hidden layer is made up of five neurons. The input to this layer is weighted and a bias is added. The connection weights are determined during training which is explained at length later in this section. The bias is used to shift the activation function. A positive value shifts the function left and a negative value shifts the function right. This too is set by the software trainer. The activation function used by the first hidden layer is a sigmoid. It determines the output activation to the second hidden

International Journal of Research
Available at https://edupediapublications.org/journals
e-ISSN: 2348-6848
p-ISSN: 2348-795X
Volume 04 Issue14
November 2017

layer. The second hidden layer has a single neuron and receives five inputs with weighted connections from the first hidden layer. The inputs are summed together by this single neuron. The activation function for the second hidden layer is linear and it determines the output activation to the output layer.The output layer processes a scalar value to propagate to the remainder of the system. After the controller interprets the data, the two ANN's produce a scalar value each that are averaged together.

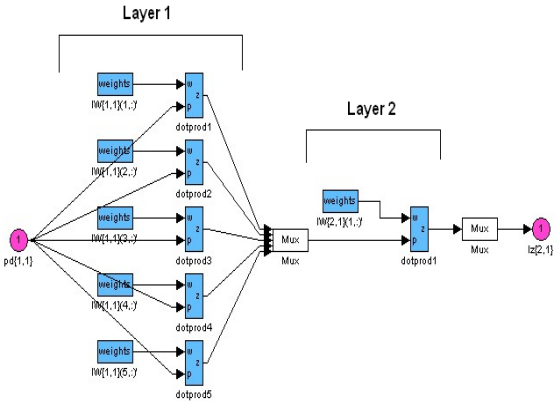

Fig. 12: Artificial Neural Network Hidden Layers

Like training in athletics, training in a neural network requires a coach, someone that describes to the neural network what it should have produced as a response. From the difference between the desired response and the actual response, the error is determined and a portion of it is propagated backward through the network. At each neuron in the network the error is used to adjust the weights and threshold values of the neuron, so that the next time, the error in the network response will be less for the same inputs.This corrective procedure is called backpropagation (hence the name of the neural network) and it is applied continuously and repetitively for each set of inputs and corresponding set of outputs produced in response to the inputs. This procedure continues so long as the individual or total errors in the responses exceed a specified level or until there are no measurable errors. At this point, the neural network has learned the training material and you can stop the training process and use the neural network to produce responses to new input data.

V. SIMULATION RESULTS

To validate the functionality of the transformerless UPFC system with proposed modulation and control algorithm, a 4160-V test setup has been developed as shown in Fig. 13(a), and the main system parameters for this test setup are given in Table III. Fig. 13(b) shows the corresponding equivalent circuit of this test setup, which is consistent with the circuit configuration shown in Fig. 2(a). In Fig. 13(b), the equivalent receiving-end voltage V_R has same amplitude as original sending-end voltage V_{S0}, but 30° phase lagging. This 30° phase lagging is introduced by transformer 2 with Y/Δ configuration (Y/Δ, 480 V/4160 V). The basic functions of the UPFC (i.e., voltage regulation, line impedance compensation, phase shifting and simultaneous control of voltage, impedance and angle) have been tested based on this setup. Some experimental results are given in this section.

A. UPFC Operation - Phase Shifting

The UPFC can function as a perfect phase angle regulator, which achieves the desired phase shift (leading or lagging) of the original sending-end voltage without any change in magnitude. Three operating points with different shifted phases are considered as shown in Fig. 14(a) case A1: 30°, (b) case A2: 15°, and (c) case A3: 0°. All three phase shifting cases (case A1 to case A3) have been tested and corresponding test results are shown in Figs. 14-17.

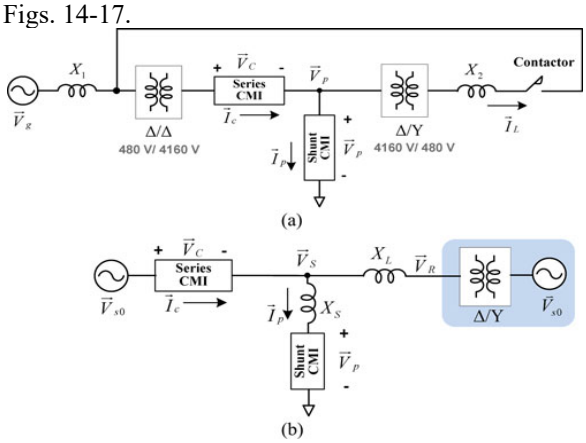

Fig. 13. 4160-V transformer less UPFC test setup.
(a) Circuit configuration and (b) corresponding equivalent circuit.

TABLE III
SYSTEM PARAMETERS FOR TEST SETUP

International Journal of Research
Available at https://edupediapublications.org/journals
e-ISSN: 2348-6848
p-ISSN: 2348-795X
Volume 04 Issue14
November 2017

Parameter	Value
Grid voltage (low voltage side) V_g	480 V
Rated frequency	60 Hz
Sampling frequency	2.5 kHz
V_{dc} of each shunt H-bridge	600 V
V_{dc} of each series H-bridge	600 V
No. of H-bridges per phase (Shunt)	6
No. of H-bridges per phase (Series)	3
Transformer 1 (Δ/Δ)	480 V/ 4160 V, 75 kVA
Transformer 2 (Y/Δ)	480 V/ 4160 V, 75 kVA
Dc capacitance of each H-bridge	2350 μF
Rated line current	10 A
Reactor X_1	2.5 mH
Reactor X_2	3.2 mH
Leakage inductance of transformer 1 (Δ/Δ)	35 mH (6% p.u.)
Leakage inductance of transformer 2 (Y/Δ)	35 mH (6% p.u.)
Equivalent line inductance X_L	0.31 H (50% p.u.)
Equivalent shunt filter inductance X_S	0.22 H (36% p.u.)

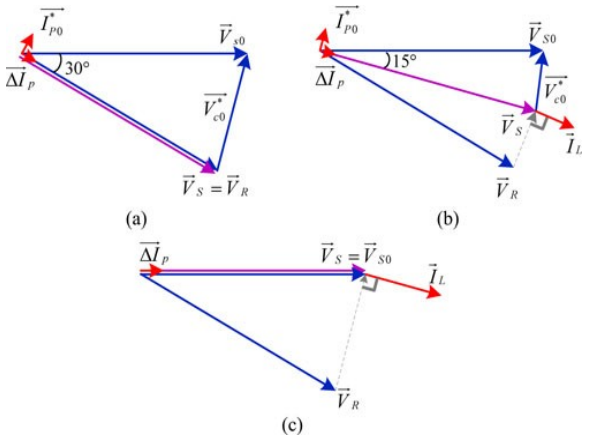

Fig. 14. UPFC operating points with different phase shifting: (a) case A1:30°, (b) case A2: 15°, and (c) case A3: 0°.

1) Fig. 15 shows the experimental waveforms of UPFC operating from case A1 to case A2 (Phase shifting 30° to 15°). As mentioned before, in the test setup, there is already 30° phase difference between the original sending-end voltage $\vec{V}_{S0}$ and the receiving-end voltage $\vec{V}_R$. For case A1, seriesCMI voltage $\vec{V}_C$ is injected to shift $\vec{V}_{S0}$ by 30° lagging, as a result, $\vec{V}_S = \vec{V}_R$. In this case, UPFC is used to compensate voltage difference caused by transformer 30° phase shift. Therefore, the resulting line current in this case is almost zero. While for case A2, new sending-end voltage $\vec{V}_S$ is shifted from $\vec{V}_{S0}$ by 15°, therefore, there is 15° phase difference between $\vec{V}_S$ and $\vec{V}_R$. This will result in about 7A (peak value) line current. Fig. 14 also shows that the current smoothly and quickly rose from zero to 7A, when the operating point is changed from case A1 to A2.

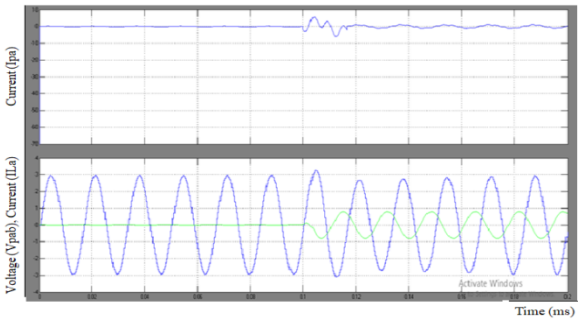

Fig. 15. Experimental waveforms of UPFC operating from case A1 to caseA2 (phase shifting 30° to 15°): line current *ILa*, shunt CMI line voltage *VP ab*, shunt CMI phase current *IP a*.

2) Similarly, the experimental waveforms of UPFC operatingfrom case A2 to case A3 (Phase shifting 15° to 0°) are shown in Fig. 16. Fig. 16(a) shows the shunt CMI phasevoltage *VP a*, *VP b* and line current *ILa*, *ILband ILc*. The *Vpa*and *Vpb* are stair-case waveforms, which are generated by the FFM with optimized switching angles. Fig. 16(b) shows the line current *ILa*and shunt CMI line voltage *VP ab*. For case A3, phase shifting is zero degree, indicating a system without compensation. Therefore, $\vec{V}_S$ is equal to $\vec{V}_{S0}$, and the phase angle between $\vec{V}_S$and $\vec{V}_R$is 30°. The resulting current amplitude in this case is 14A.

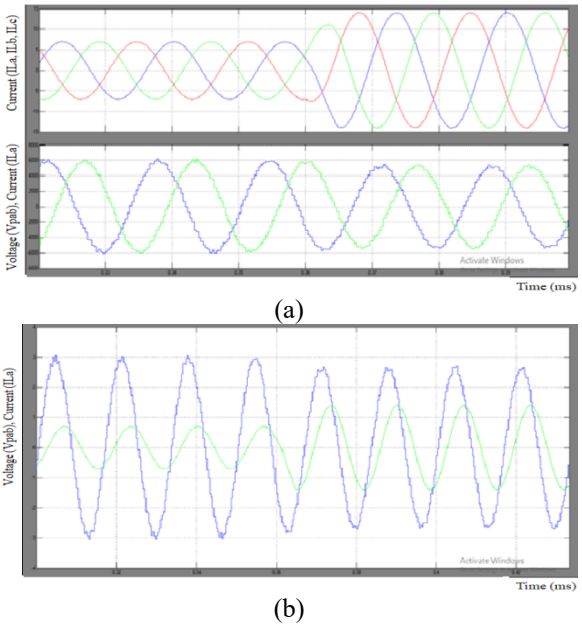

Fig. 16. Experimental waveforms of UPFC operating from case A2 to caseA3 (phase shifting 15° to 0°): (a) shunt CMI phase voltage *VP a* ,*VP b* and line current *ILa* , *ILb* , *ILc* , and (b) line current *ILa* and shunt CMI line voltage *VP ab* .

International Journal of Research
Available at https://edupediapublications.org/journals
e-ISSN: 2348-6848
p-ISSN: 2348-795X
Volume 04 Issue14
November 2017

3) Fig. 17 shows the measured dynamic response with operating point changing from case A2 to case A3, where the current amplitude would change from 7 to 14 A. Since the system dynamic model has been included in the control algorithm as shown in Fig. 8, the UPFC system has achieved fast dynamic response, with response time <10ms. This dynamic performance is good enough for transmission-level power flow control.

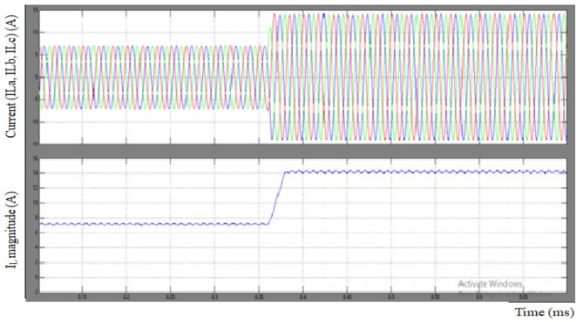

Fig. 17. Measured dynamic response with operating point changing from caseA2 to case A3 (phase shifting 15° to 0°).

4) Fig. 18 shows the experimental results of dc capacitorvoltage of both series and shunt CMIs when operating from case A2 to case A3, where top three waveforms correspond to average dc voltage of each phase, and bottom one corresponds to average dc voltage of all three phases. During the transition, the dc link voltage almost kept constant, which means the dc link voltage can be controlled to follow the reference faithfully regardless of operating points.

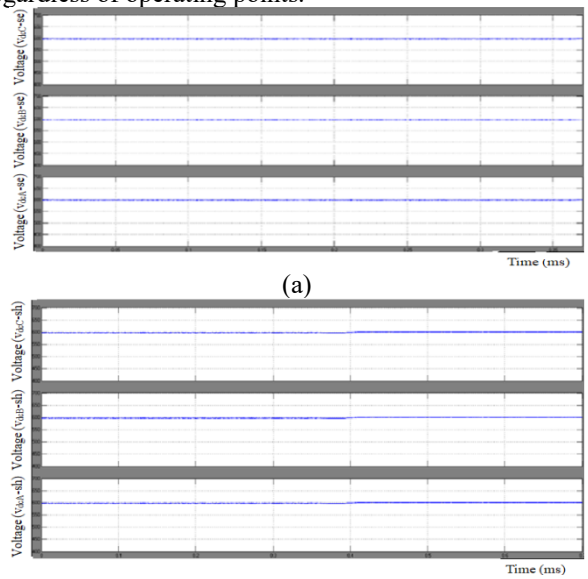

Fig. 18. Experimental results of dc capacitor voltage of series and shunt CMIs,from case A2 to case A3 (phase shifting 15° to 0°): (a) dc capacitor voltage of series CMI and (b) dc capacitor voltage of shunt CMI.

B. UPFC Operation - Line Impedance Compensation

UPFC function of line impedance compensation is different from phase shifting, where the series CMI voltage $\vec{V}_c$ is injectedin quadrature with the line current. Functionally it is similar to series capacitive or inductive line compensation attained by static synchronous series compensator. Fig. 19 shows three operation points with line impedance compensation, (a) caseB1: original line impedance without compensation is equal to 0.5p.u.,(b) case B2: equivalent line impedance after compensation is equal to 1p.u., and (c) case B3: equivalent line impedance after compensation is equal to infinity. For case B1 (same as case A3), system without compensation has 0.5p.u. voltage between $\vec{V}_S$ and $\vec{V}_R$ (corresponding to 30° voltage difference). With the line impedance equal to 0.31 H (0.5p.u.) given in Table III, the resulted line current is 1p.u. (amplitude 14 A), which is the nominal current for transformer 1 and transformer 2 in the 4160-V test setup. Due to the current limitation of transformers, for case B2 and case B3, UPFC is purposely controlled to increase the line impedance. Nevertheless, the transformer less UPFC is also able to reduce the line impedance for higher line current (or higher P/Q).

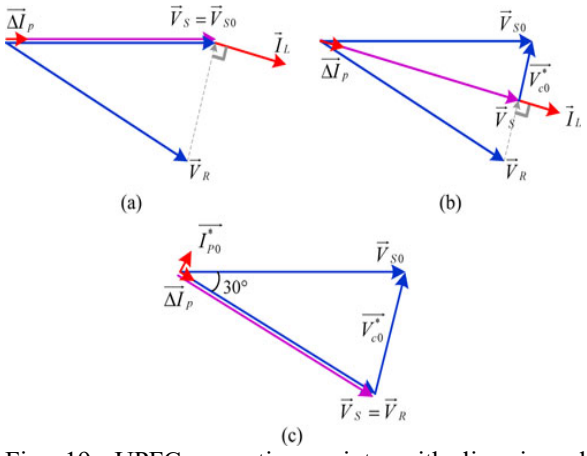

Fig. 19. UPFC operating points with line impedance compensation: (a) case B1: original line impedance without compensation = 0.5p.u., (b) case B2: equivalent line impedance after compensation =1p.u., and (c) case B3: equivalent line impedance after compensation = ∞.

Fig. 20 shows the experimental results of UPFC operation from case B1 to case B2, where the line impedance changedfrom original 0.5p.u. without compensation to 1p.u. after compensation. Fig. 19(a) shows the waveforms of shunt CMI phase voltage V_{Pa}, V_{Pb} and line current I_{La}, I_{Lb}, I_{Lc}, where the line current

International Journal of Research
Available at https://edupediapublications.org/journals
e-ISSN: 2348-6848
p-ISSN: 2348-795X
Volume 04 Issue14
November 2017

smoothly changed from 14 to 7 A (peak value) due to the doubled line impedance. Fig. 19(b) shows the waveforms of the series CMI injected voltage V_{Ca} and line current I_{La}. From this figure, we can see the line current I_{la} is lagging V_{Ca} by 90°, which means the series CMIs act as inductors. This is the reason that, after compensation, the line impedance is increased from 0.5 to 1p.u. Fig. 21shows the dynamic response with operating point changing from case B1 to case B2. The measured response time is about 6ms.

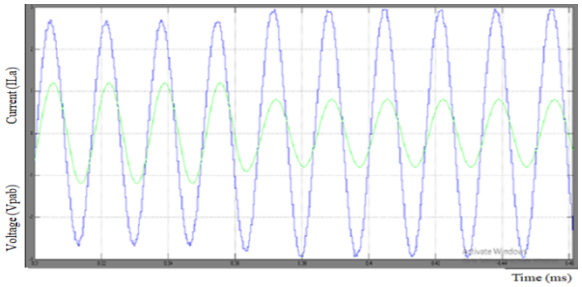

(a)

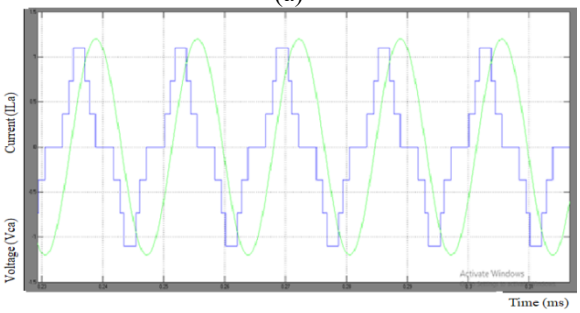

(b)

Fig. 20. Experimental waveforms of UPFC operating from case B1 to caseB2 (line impedance from original 0.5p.u. without compensation to 1p.u. after compensation): (a) line current *ILa* and shunt CMI line voltage *VP ab* , (b) line current *ILa* and series CMI phase voltage *VC a* .

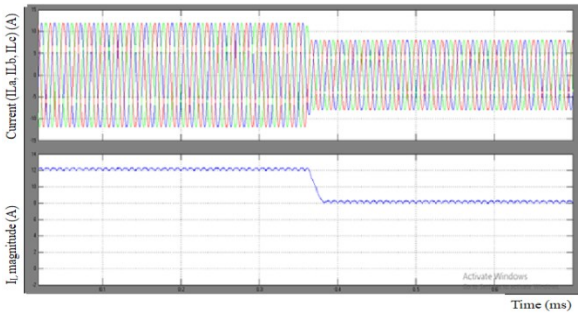

Fig. 21. Measured dynamic response with operating point changing from case B1 to case B2 (line impedance from original 0.5p.u. without compensation to 1p.u. after compensation).

C. UPFC Operation - Independent P/Q Control

The functions of voltage regulation, phase shifting and line impedance compensation are from the standpoint of traditional power transmission control. Actually, the UPFC can simply control the magnitude and phase angle of the injected voltage in real time so as to maintain or vary the active and reactive power flow in the line to satisfy load demand and system operating conditions, i.e., independent *P/Q* control.

The blue curve in Fig. 22(a) shows the transmittable active power P and receiving-end reactive power Q versus receiving end voltage phase angle $\delta 0$ in the uncompensated system, where original sending-end voltage is oriented to 0°. The circle in Fig. 22(a) shows the control region of the attainable active power and receiving-end reactive power with series CMI voltage equal to 0.517p.u. and phase angle $\delta 0$ equal to -30°. In general, at any given $\delta 0$, the transmitted active power P as well as receiving end reactive power Q within the circle can be controlled by the UPFC, of course, with the rating limitation of series and shunt CMIs [28]. Several operating points of independent *P/Q* control have been tested.

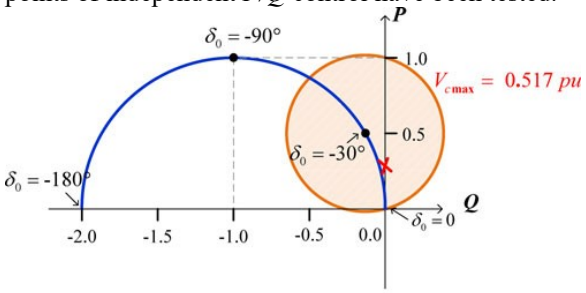

(a)

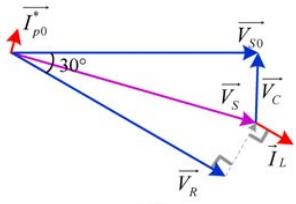

(b)

Fig. 21. Independent *P/Q* control: (a) control region of the attainable active power P and receiving-end reactive power Q with series CMI voltage = 0.517p.u. and$\delta 0 = -30^{\circ}$, (b) case C1: $P = 0.25$, $Q = 0$.

Fig. 22(b) shows the phasor diagram for one of the test cases, case C1: $P = 0.25$, $Q = 0$, in this case, line current$\vec{I}_L$is in phase with receiving-end voltage$\vec{V}_R$due to zero receiving-end reactive power Q. In this case, the calculated line current amplitude is 7.5 A.

International Journal of Research
Available at https://edupediapublications.org/journals
e-ISSN: 2348-6848
p-ISSN: 2348-795X
Volume 04 Issue14
November 2017

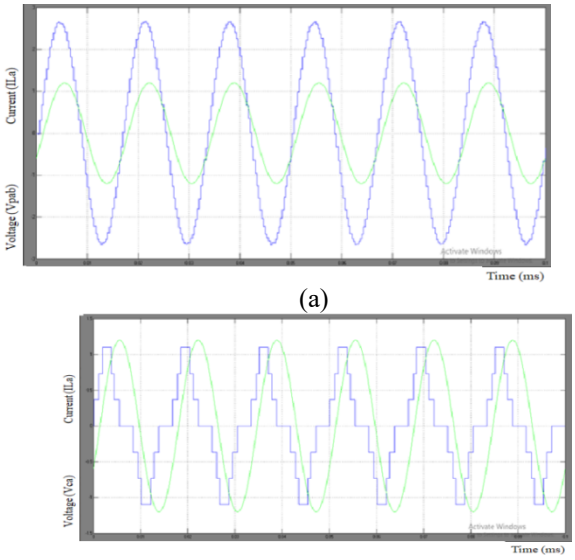

Fig. 23.Experimental waveforms of UPFC operation case C1: $P = 0.25, Q = 0$: (a) line current *ILa* and shunt CMI line voltage *VP ab* , and (b) line current *ILa* and series CMI phase voltage *VC a* .

TABLE II
COMPARISON OF THD VALUES

CASE	Without ANN	With ANN
From case A1 to case A2	6.13%	3.45%
From case A2 to case A3	6.15%	4.41%
From case B1 to case B2	6.13%	3.65%
In case C1	6.18%	4.18%

VI. CONCLUSION

According to this paper, we present a modulation and new control technique for the transformer less UPFC, which has the subsequent features: All UPFC functions, together with voltage law, line impedance reimbursement, segment transferring or simultaneous manipulate of voltage, impedance, and section attitude, thus attaining unbiased energetic and reactive electricity drift manage over the transmission line; By adding the new ANN control technique to the system for controlling, it provides us low THD values as show in TABLE II; Dc capacitor voltage balancing control for both series and shunt; Fast dynamic response. The transformerless UPFC with proposed modulation and control technique may be mounted everywhere in the grid to maximize and optimize electricity transmission over the prevailing grids, reduce transmission congestion and enable high penetration of renewable electricity resources if the practical ANN system is designed for operation, which is under enormous study for practical designing and application.

REFERENCES

[1] N. G. Hingorani and L. Gyugyi, Understanding Facts: Concept and Technology of Flexible AC Transmission Systems. Piscataway, NJ, USA: IEEE Press, 2000.

[2] L.Gyugyi, C.D. Schauder, S. L.Williams, T. R. Rietman, D. R. Torgerson, and A. Edris, "The unified power flow controller: A new approach to power transmission control," IEEE Trans. Power Del., vol. 10, no. 2, pp. 1085– 1097, Apr. 1995.

[3] A. Rajabi-Ghahnavieh, M. Fotuhi-Firuzabad, M. Shahidehpour, and R. Feuillet, "UPFC for enhancing power system reliability," IEEE Trans. Power Del., vol. 25, no. 4, pp. 2881–2890, Oct. 2010.

[4] H. Fujita, Y. Watanabe, and H. Akagi, "Control and analysis of a unified power flow controller," IEEE Trans. Power Electron., vol. 14, no. 6, pp. 1021–1027, Nov. 1999.

[5] M. A. Sayed and T. Takeshita, "Line loss minimization in isolated substations and multiple loop distribution systems using the UPFC," IEEE Trans. Power Electron., vol. 29, no. 11, pp. 5813–5822, Jul. 2014.

[6] H. Fujita, Y. Watanable, and H. Akagi, "Transient analysis of a unified power flow controller and its application to design of dc-link capacitor," IEEE Trans. Power Electron., vol. 16, no. 5, pp. 735–740, Sep. 2001.

[7] H. Fujita, H. Akagi, and Y. Watanable, "Dynamic control and performance of a unified power flow controller for stabilizing an AC transmission system," IEEE Trans. Power Electron., vol. 21, no. 4, pp. 1013–1020, Jul. 2006.

[8] L. Liu, P. Zhu, Y. Kang, and J. Chen, "Power-flow control performance analysis of a unified power-flow controller in a novel control scheme," IEEE Trans. Power Del., vol. 22, no. 3, pp. 1613–1619, Jul. 2007.

[9] S. Kanna, S. Jayaram, and M. M. A. Salama, "Real and reactive power coordination for a unified power flow controller," IEEE Trans. Power Syst., vol. 19, no. 3, pp. 1454–1461, Aug. 2004.

[10] J. Z. Bebic, P. W. Lehn, and M. R. Iravani, "P-Δ characteristics for the unified power flow controller - Analysis inclusive of equipment ratings and line limits," IEEE Trans. Power Del., vol. 18, no. 3, pp. 1066–1072, Jul. 2003.

[11] C. D. Schauder, L. Gyugyi, M. R. Lund, D. M. Hamai, T. R. Rietman, D. R. Torgerson, and A. Edris, "Operation of the unified power flow controller (UPFC) under practical constraints," *IEEE Trans. Power Del.*, vol. 13, no. 2, pp. 630–639, Apr. 1998.

[12] S. Y. Kim, J. S. Yoon, B. H. Chang, and D. H. Baek, "The operation experience of KEPCO UPFC," in *Proc. 8th Int. Conf. Electr. Mach. Syst.*, 2005, pp. 2502–2505.
[13] C. Schauder, E. Stacey, M. Lund, L. Gyugyi, L. Kovalsky, A. Keri,A. Mehraban, and A. Edris, "AEP UPFC project: Installation, commissioningand operation of the 160MVA STATCOM (phase I)," *IEEE Trans. Power Del.*, vol. 13, no. 4, pp. 1530 1535, Oct. 1998.
[14] K. Sano and M. Takasaki, "A transformer less D-STATCOM based on amulti voltage cascade converter requiring no DC sources," *IEEE Trans.Power Electron.*, vol. 27, no. 6, pp. 2783–2795, Jun.2012.
[15] B. A. Renz, A. Keri, A. S. Mehraban, C. Schauder, E. Stacey,L. Kovalsky, L. Gyugyi, and A. Edris, "AEP unified power flow controllerperformance," *IEEE Trans. Power Del.*, vol. 14, no. 4, pp. 1374–1381,Oct. 1999.
[16] J. Monteiro, J. F. Silva, S. F. Pinto, and J. Palma, "Matrix converter-basedunified power-flow controllers: Advanced direct power control method,"*IEEE Trans. Power Del.*, vol. 26, no. 1, pp. 420–430, Jan. 2011.
[17] J. Monteiro, J. F. Silva, S. F. Pinto, and J. Palma, "Linear and sliding-modecontrol design for matrix converter-based unified power flow controllers,"*IEEE Trans. Power Electron.*, vol. 29, no. 7, pp. 3357–3367, Jul. 2014.
[18] A. Dasgupta, P. Tripathy, and P. S. Sensarma, "Matrix converter as UPFC for transmission line compensation," in *Proc. Int. Conf. Power Electron.*, Oct. 2007, pp. 1050–1055.
[19] Z. Yuan, S. W. H. de Haan, J. B. Ferreira, and D. Cvoric, "A FACTS device: Distributed power flow controller (DPFC)," *IEEE Trans. Power Electron.*, vol. 25, no. 10, pp. 2564–2572, Oct. 2010.
[20] F. Z.Peng and J. Wang, "A universal STATCOM with delta-connectedcascade multilevel inverter," in *Proc. Annu. IEEE Power Electron. Spec.Conf.*, 2004, pp. 3529–3533.
[21] F. Z. Peng, J. S. Lai, J.W. McKeever, and J. Van Coevering, "A multilevelvoltage-source inverter with separate dc sources for static var generation,"*IEEE Trans. Ind. Appl.*, vol. 32, no. 5, pp. 1130 1138, Sep. 1996.
[22] F. Z. Peng and J. S. Lai, "Dynamic performance and control of a staticvar generator using cascade multilevel inverters," *IEEE Trans. Ind. Appl.*,vol. 33, no. 3, pp. 748–755, May/Jun. 1997.
[23] H. Akagi, S. Inoue, and T. Yoshii, "Control and performance of a transformerlesscascade PWM STATCOMwith star configuration," *IEEE Trans.Ind. Appl.*, vol. 43, no. 4, pp. 1041–1049, Jul./Aug. 2007.
[24] B. Gultekin, C. O. Gercek, T. Atalik, M. Deniz, N. Bicer, M. Ermis,K. N. Kose, C. Ermis, E. Koc, I. Cadirci, A. Acik, Y. Akkaya, H. Toygar,and S.Bideci, "Design and implementation of a 154-kV 50-Mvar transmissionSTATCOM based on 21-level cascaded multilevel converter," *IEEETrans. Ind. Appl.*, vol. 48, no. 3, pp. 1030–1045, May/Jun. 2012.
[25] B. Gultekin and M. Ermis, "Cascaded multilevel converter-based transmissionSTATCOM: System design methodology and development of a12 kV 12 MVAr power stage," *IEEE Trans. Power Electron.*, vol. 28,no. 11, pp. 4930–4950, Nov. 2013.
[26] J. Wang and F. Z. Peng, "Unified power flow controller using the cascademultilevel inverter," *IEEE Trans. Power Electron.*, vol. 19, no. 4,pp. 1077–1084, Jul. 2004.
[27] F. Z. Peng, S. Zhang, S. T. Yang, G. Deepak, and K. Ujjwal, "Transformerlessunified power flow controller using the cascade multilevel inverter,"in *Proc. Int. Power Electron. Conf.*, 2014, pp. 1342 1349.
[28] H., Symon, (2005) Neural Networks: A Comprehensive Foundation 2nd edition PHI Publication, New Delhi, India.
[29] D. Niebur and T.S. Dillon, (1996) Neural Network Applications in Power Systems CRL Publishing Ltd. U.K.
[30] H. Hussain Mohamed, (1998) Fundamentals of Artificial Neural networks PHI publication, New Delhi.
[31] Sasaki, H., Watanabe, M., and Yokohama, R. (1992) A solution method of unit commitment by artificial neural networks IEEE trans. Power Syst., 7(3), pp. 974-980.

AUTHOR'S PROFILE:

B. Divya Sree is currently working as MATLAB developer and Branch Manager (DSNR) in VISION KREST EMBEDDED TECHNOLOGIES, Private Ltd., Hyderabad. She received her Master of Technology degree in ELECTRICAL POWER ENGINEERING from CVR College of Engineering, Ibrahimpatnam, Hyderabad, Telangana; she received her Bachelor of Engineering degree from Vijay College of Engineering for women, Nizamabad. Her areas of interest are Electrical Power Systems, Power Electronics and FACTS.

Email id: divyasrees.balipogula@gmail.com